

# Tandem Catalysis by Palladium Nanoclusters Encapsulated in Metal–Organic Frameworks

Xinle Li,<sup>‡,†,§</sup> Zhiyong Guo,<sup>‡,†,§</sup> Chaoxian Xiao,<sup>†,§</sup> Tian Wei Goh,<sup>†,§</sup> Daniel Tesfagaber,<sup>†,§</sup> and Wenyu Huang<sup>\*,†,§</sup>

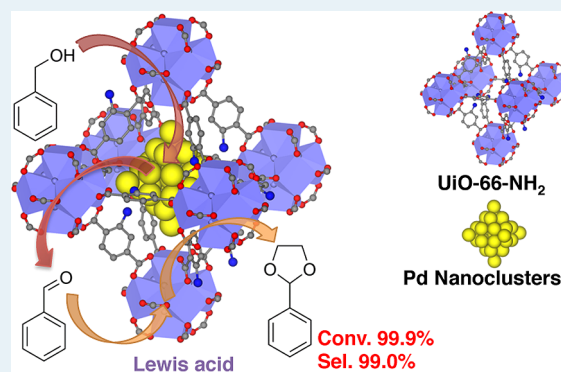
<sup>‡</sup>Department of Chemistry, Iowa State University, Ames, Iowa 50011, United States

<sup>§</sup>Ames Laboratory, USDOE, Ames, Iowa 50011, United States

## S Supporting Information

**ABSTRACT:** A bifunctional Zr-MOF catalyst containing palladium nanoclusters (NCs) has been developed. The formation of Pd NCs was confirmed by transmission electron microscopy (TEM) and extended X-ray absorption fine structure (EXAFS). Combining the oxidation activity of Pd NCs and the acetalization activity of the Lewis acid sites in UiO-66-NH<sub>2</sub>, this catalyst (Pd@UiO-66-NH<sub>2</sub>) exhibits excellent catalytic activity and selectivity in a one-pot tandem oxidation-acetalization reaction. This catalyst shows 99.9% selectivity to benzaldehyde ethylene acetal in the tandem reaction of benzyl alcohol and ethylene glycol at 99.9% conversion of benzyl alcohol. We also examined various substituted benzyl alcohols and found that alcohols with electron-donating groups showed better conversion and selectivity compared to those with electron-withdrawing groups. We further proved that there was no leaching of active catalytic species during the reaction and the catalyst can be recycled at least five times without significant deactivation.

**KEYWORDS:** tandem synthesis, acetalization, bifunctional catalysts, UiO-66, acetal, solid acid, selective oxidation



## 1. INTRODUCTION

With the pressing need for catalysis technologies that could address the energy crisis and environmental pollution confronting our societies, a great deal of research effort has been devoted to finding novel and efficient multifunctional catalysts for one-pot tandem reactions.<sup>1–8</sup> Tandem catalysis, in which multistep chemical transformations are catalyzed with a multifunctional catalyst, has attracted increasing research attention because selective multifunctional catalysts will make a multistep reaction go to the desired products in one reactor without the need for separation, purification, and transfer of intermediates produced in each step. The development of multistep catalytic processes using multifunctional catalysts can also minimize the amount of byproducts/waste produced during multistep chemical reactions and achieve atomic efficiency, one of the focuses of green chemistry. Conversely, traditional multistep catalytic processes involve a series of conversions in different reactors with intermediate purification steps to achieve a desired product. Therefore, traditional multistep catalytic processes usually require a high-energy input for the separation of intermediates and cause low yield of the final products due to the losses of intermediates within each individual step of the processes.

Metal–organic frameworks (MOFs), a class of porous materials assembled from metal ions/clusters and organic ligands, have been investigated extensively because of their high

surface areas, well-defined porosities, and chemical tenability.<sup>9</sup> MOFs have been utilized for many applications including gas storage, separations, chemical sensing, and drug delivery.<sup>10–13</sup> In recent years, MOFs have demonstrated their potential application as heterogeneous catalysts, especially those using MOFs as a supporting matrix for metal nanoparticles (known as metal@MOFs).<sup>14–23</sup> Despite the many investigations of the MOFs' role in catalysis, there are only a limited number of studies of bifunctional metal@MOFs systems for tandem catalysis. Fischer et al. and Haruta et al. reported Au@ZIF-8 and Au@MOF-5 as catalyst in the synthesis of methyl benzoate from the aerobic oxidation of benzyl alcohol, respectively;<sup>24,25</sup> Corma et al. developed Pd@MIL-101 as a catalyst for one-pot synthesis of menthol from citronellal.<sup>26</sup> Li's group prepared Pd@MIL-101 for the one-pot synthesis of methyl isobutyl ketone from acetone.<sup>27</sup> Recently, Li's group also prepared a bimetallic MOF catalyst (Au–Pd@MIL-101) and used it for the one-pot synthesis of aromatic esters from alkyl aromatics.<sup>28,29</sup> Tang et al. designed a core–shell Pd@IRMOF-3 and used it as a multifunctional catalyst for a cascade condensation-hydrogenation reaction.<sup>30</sup>

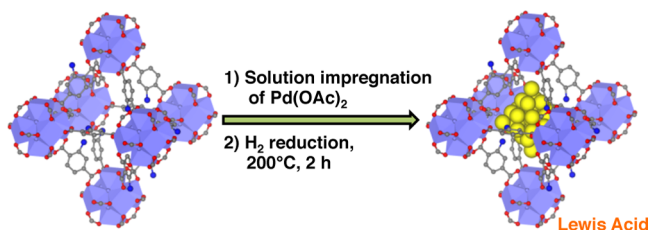
Received: May 14, 2014

Revised: August 22, 2014

Published: August 25, 2014

As pointed out by recent reviews, the field of developing tandem catalysis using MOFs remains relatively unexplored and will have a large impact on current industrial processes.<sup>31</sup> Herein, we developed a bifunctional tandem heterogeneous catalyst by encapsulating Pd nanoclusters (NCs) in the cavities of UiO-66-NH<sub>2</sub> (Scheme 1), which could catalyze the oxidation

**Scheme 1. Synthesis of the Heterogeneous Tandem Catalyst by Encapsulating Pd NCs Inside the Cavities of UiO-66-NH<sub>2</sub>**



of benzyl alcohol and the subsequent acetalization of benzaldehyde with ethylene glycol. To the best of our knowledge, this is the first example of applying MOF-based heterogeneous catalysts in tandem oxidation-acetalization reaction in liquid phase. One-pot tandem reaction through oxidation of alcohols followed by acetalization of the carbonyl compounds using heterogeneous catalysts in liquid phase has rarely been studied so far. Considerable research aiming at one-step gas phase conversion of methanol to 1,1-dimethoxy-methane over a variety of heterogeneous catalytic systems can be found in the literature, that is, molybdenum-based catalysts,<sup>32</sup> heteropoly acids (HPAs),<sup>33</sup> oxides of ruthenium and rhenium,<sup>34–37</sup> as well as vanadium-based catalysts.<sup>38–40</sup> With regard to one-pot higher acetals synthesis, we only found limited work related to the direct synthesis from ethanol via photocatalytic oxidation or H<sub>2</sub>O<sub>2</sub> oxidation catalyzed by Fe (III) complexes.<sup>41–43</sup> Two combined catalytic systems, Pd(OAc)<sub>2</sub>/Cu(OAc)<sub>2</sub>/*p*-toluenesulfonic acid<sup>44</sup> and manganese dioxide/trialkyl orthoformate/indium triflate,<sup>45</sup> also showed activity in tandem oxidation/acetalization reactions.

UiO-66-NH<sub>2</sub> is built up from [Zr<sub>6</sub>O<sub>4</sub>(OH)<sub>4</sub>(CO<sub>2</sub>)<sub>12</sub>] clusters linked with 2-aminoterephthalic acid.<sup>46</sup> UiO-66-NH<sub>2</sub> possesses uncoordinated zirconium sites, which could serve as Lewis acid sites for catalysis. These Lewis acid sites have been used to catalyze the cross-aldol condensation, cyclization of citronellal, and acetalization.<sup>47–49</sup> By combining the oxidation activity of Pd NCs and the acetalization activity of the Lewis acid sites on UiO-66-NH<sub>2</sub>, we developed this tandem Pd@UiO-66-NH<sub>2</sub> catalyst, which showed 99.9% conversion of benzyl alcohol in the one-pot tandem reaction of benzyl alcohol and ethylene glycol with 99.9% acetal selectivity. Acetals are a class of chemicals that can be used for the protection of carbonyl compounds. They are also widely utilized as organic solvents, fuel additives, steroids, besides being important in the pharmaceutical and fragrance industries.<sup>50,51</sup> Generally, acetal synthesis is carried out by the condensation of alcohols with aldehydes using mineral acid catalysts.<sup>52</sup> However, these catalysts are toxic, corrosive, and difficult to be removed after the reaction.

## 2. EXPERIMENTAL SECTION

**2.1. Materials and Synthesis.** *Synthesis of UiO-66-NH<sub>2</sub> and UiO-66.* The MOF was synthesized and purified according to a procedure reported by Lillerud and co-workers.<sup>53</sup> For UiO-

66-NH<sub>2</sub>, zirconium(IV) chloride (0.40 g, 1.71 mmol; 98%, Acros Organics) and 2-aminoterephthalic acid (NH<sub>2</sub>-H<sub>2</sub>BDC) (0.31 g, 1.71 mmol; >99%, Sigma-Aldrich) were dissolved in 100 mL of *N,N'*-dimethylformamide (DMF; ACS grade, Macron) at room temperature, and then 140 μL of water was added. For UiO-66, terephthalic acid (0.29 g, 1.71 mmol; 98%, Sigma-Aldrich) was used as the organic linker, and no water was added during the synthesis. The obtained mixture was sealed and placed in a preheated oven at 120 °C for 24 h. The solid MOFs were washed with fresh DMF, chloroform, and methanol three times every 12 h. Then it was activated at 150 °C under vacuum (30 mTorr) for 6 h.

*Synthesis of Pd NCs Inside the Cavities of UiO-66-NH<sub>2</sub> and UiO-66.* UiO-66-NH<sub>2</sub> (100 mg) was dispersed in 12 mL of methylene chloride (Fisher, Optima grade). After sonication for 1 h, a methylene chloride solution of palladium acetate (4.32 mg Pd(OAc)<sub>2</sub> in 5 mL of methylene chloride, Kawaken Fine Chemicals) was added dropwise to the MOF solution under vigorous stirring. After 24 h of stirring at room temperature, the as-prepared Pd<sup>2+</sup> infiltrated MOF was washed three times for 12 h each time with fresh methylene chloride. The reduction process of the precursor loaded UiO-66-NH<sub>2</sub> was performed under a 50 mL/min flow of 10% H<sub>2</sub>/Ar at 200 °C for 2 h. The same method was used to synthesize Pd NCs inside UiO-66.

**2.2. Instrumentation.** *BET, PXRD, TEM, XPS, and TGA.* Surface area analysis of the catalyst was performed by nitrogen sorption isotherms in a Micromeritics Tristar 3000 surface area analyzer at 77 K. Powder X-ray diffraction (PXRD) patterns of the samples were obtained by a STOE Stadi P powder diffractometer using Cu Kα radiation (40 kV, 40 mA, λ = 0.1541 nm). The size and morphology of 2.0 wt % Pd@UiO-66-NH<sub>2</sub> were investigated by using transmission electron microscopy (TEM) and high-angle annular dark-field scanning transmission electron microscopy (HAADF-STEM) images recorded on a Tecnai G2 F20 electron microscope equipped with an energy-dispersive X-ray (EDX) detector (Oxford INCA EDS). X-ray photoelectron spectroscopy (XPS) measurements were performed using a PHI 5500 Multitechnique system (Physical Electronics, Chanhassen, MN) with a monochromatized Al Kα X-ray source (hν = 1486.6 eV). Thermogravimetric analysis (TGA) was carried out using STA 6000 simultaneous thermal analyzer (PerkinElmer). In the TGA experiment, 5.7 mg of Pd@UiO-66-NH<sub>2</sub> was analyzed under N<sub>2</sub> flow with a heating rate of 10 °C/min from room temperature to 900 °C.

*Inductively Coupled Plasma Atomic Emission Spectroscopy (ICP-AES).* To determine the loading amount of palladium in UiO-66-NH<sub>2</sub>, ICP-AES (Optima 2100 DV) was performed. Because the zirconium in UiO-66-NH<sub>2</sub> has similar emission with palladium in ICP-AES, it is difficult to detect the palladium amount directly. Instead, we measured the amount of Pd that was washed away during the washing steps and calculated the actual Pd remaining in Pd@UiO-66-NH<sub>2</sub>. When loading the 2.0 wt % Pd in UiO-66-NH<sub>2</sub>, the exact initial weight of the palladium precursor (palladium acetate) was recorded first. Every time after washing, the washing solution that contained the palladium acetate residue was collected. Finally, ICP-AES was performed for the washing solution, and the palladium content was calculated. The difference between added and removed Pd (during washing) is the actual palladium amount that was loaded in UiO-66-NH<sub>2</sub>. The same method was also used to determine the actual Pd amount in Pd@UiO-66.

**Extended X-ray Absorption Fine Structure (EXAFS).** The EXAFS spectra were measured in transmission mode (Pd K edge = 24.350 keV) at 20-BM-B and 9-BM-B beamlines of the Advanced Photon Source at Argonne National Laboratory. EXAFS of reference samples were collected using pure finely ground powders homogeneously dispersed on polyimide Kapton tap, whereas the MOF samples were pressed into a pellet fit to a hole embedded in a Teflon substrate. A palladium foil spectrum was acquired simultaneously with each measurement for energy calibration. Multiple scans (8–10 scans) were collected for each sample, and merged into one data set for EXAFS analysis. For the analysis, the software at the beamlines was used to perform dead-time correction, and energy calibration. The Athena program, which is an interface to IFEFFIT package, was used for glitch removal, pre-edge subtraction, postedge normalization, and conversion to  $k$ -space.<sup>54,55</sup> The EXAFS data were fitted in  $R$ -space using the Artemis program from the same package, with theoretical models constructed from FEFF6.<sup>56–58</sup> All the EXAFS data fitting were performed with a  $k^3$  weighting in  $R$ -space. The  $k$  ranges ( $\text{\AA}^{-1}$ ),  $R$ -ranges, independent points in the EXAFS spectrum, the number of variables determined in the models, and the fitting quality are given in Supporting Information, Table S2.

**2.3. Catalysis.** The tandem reaction was carried out under reflux in a 10 mL round-bottom flask equipped with a condenser whose temperature was maintained at 5 °C using a recirculating chiller (NESLAB, R134A). In a typical catalytic measurement, 10.5 mg of benzyl alcohol (0.1 mmol, Fisher Scientific), 100  $\mu\text{L}$  of ethylene glycol (Fisher Scientific), 5.0 mg of 2.0 wt % Pd@UiO-66-NH<sub>2</sub> (1 mol %), and 7 mg of mesitylene (internal standard, 99%, Acros Organics) were added into 2 mL of cyclohexane in the round-bottom flask. An oxygen balloon at the top of the condenser was used to supply oxygen for the reaction. The flask was loaded in an oil bath that was preheated to 90 °C. The reaction was kept under reflux with magnetic stirring at 600 rpm for designated time. After the reaction was finished, the products were analyzed using a gas chromatograph (GC) equipped with a HP-5 capillary column (30 m  $\times$  0.32 mm  $\times$  0.25  $\mu\text{m}$ ) and a flame ionization detector. The products were identified by a GC-MS (SHIMADZU 5050A) equipped with a HP-5ms capillary column (30 m  $\times$  0.25 mm  $\times$  0.25  $\mu\text{m}$ ).

**Recycling Test.** The catalyst was isolated at the end of the reaction and the liquid was removed. The solid catalyst was reused in the second run. The catalytic activity and acetal selectivity of the catalyst did not show significant loss in the second run. PXRD of the used sample showed that the structure of the catalyst remained intact during the catalytic cycles. The Pd@UiO-66-NH<sub>2</sub> catalyst did not show any deactivation within five cycles of the reaction.

**Leaching Test.** The solid catalyst (Pd@UiO-66-NH<sub>2</sub>) was separated from the hot solution right after reaction for 90 min. The reaction was continued with the filtrate in the absence of solid catalyst for an additional 8 h. No further increase in either the conversion of benzyl alcohol or the selectivity of acetal was observed, which indicates that the catalytically active sites for both oxidation and acetalization are on the solid catalyst.

### 3. RESULTS AND DISCUSSION

**3.1. Synthesis and Characterization.** The Pd@UiO-66-NH<sub>2</sub> catalyst was synthesized by loading Pd precursor, palladium(II) acetate, into UiO-66-NH<sub>2</sub> in methylene chloride.

After separating the MOF powder by centrifugation, we dried the powder under vacuum at 80 °C and then reduced the Pd(II) loaded MOF under 50 mL/min flow of 10% H<sub>2</sub>/Ar at 200 °C to form Pd NCs (Scheme 1). The successful loading of Pd in UiO-66-NH<sub>2</sub> was confirmed by EDX spectroscopy. As shown in Figure S1 (Supporting Information), a clear Pd peak was resolved when we probed selected area 1 on the Pd loaded MOF. We also observed a similar EDX spectrum when we probed area 2. The loading of Pd in UiO-66-NH<sub>2</sub> is 2.0 wt % measured by inductively coupled plasma atomic emission spectroscopy (ICP-AES).

The transmission electron microscopy (TEM) image of Pd@UiO-66-NH<sub>2</sub> is shown in Figure 1a, in which Pd NCs are well

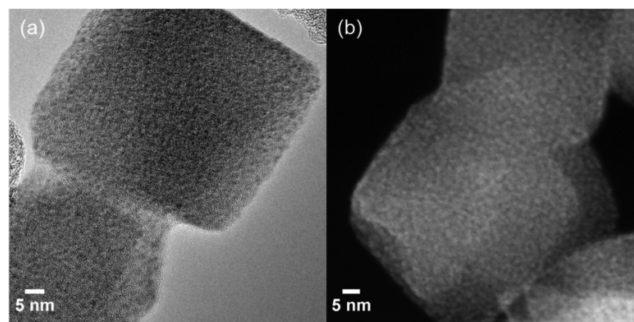


**Figure 1.** (a) TEM and (b) HAADF-STEM images of 2.0 wt % Pd@UiO-66-NH<sub>2</sub>. The Pd@UiO-66-NH<sub>2</sub> was synthesized by loading Pd precursor, palladium(II) acetate, into UiO-66-NH<sub>2</sub> in CH<sub>2</sub>Cl<sub>2</sub>. After separating and drying the powder, we reduced it under 50 mL/min flow of 10% H<sub>2</sub>/Ar at 200 °C to form Pd NCs.

dispersed with a mean diameter less than 1.2 nm (the diameter of the large octahedral cages in UiO-66-NH<sub>2</sub>). To increase the contrast of the Pd NCs against the MOF support, we also measured high-angle annular dark-field scanning transmission electron microscopy (HAADF-STEM) images of Pd@UiO-66-NH<sub>2</sub> as shown in Figure 1b. We could not find any particle that has a diameter larger than 1.2 nm, which indicates that the formed Pd NCs are well-dispersed inside the cavities of the MOF. From the EDX mapping of selected area on the Pd@UiO-66-NH<sub>2</sub> (the rectangle indicated by the dashed line in Supporting Information, Figure S2a), Pd was found to exist along with Zr as shown in Supporting Information, Figure S2b,c, indicating Pd was effectively trapped by the MOF. The dispersion was uniform, and no sign of aggregation was observed. We are aware that the 2D TEM images cannot exclusively determine whether the Pd NCs are located inside or on the surface of the MOF. Therefore, we tried to rotate the TEM sample and track the same Pd NCs to confirm that these NCs are located inside the MOF. Using this method, we were able to confirm that Pt NCs are encapsulated in UiO-66-NH<sub>2</sub>.<sup>59</sup> However, to follow the same Pd NC is extremely hard during the TEM measurement because of the small difference in electron beam contrast for Pd NCs and [Zr<sub>6</sub>O<sub>4</sub>(OH)<sub>4</sub>(CO<sub>2</sub>)<sub>12</sub>] clusters in the MOF.

PXRD pattern of as-synthesized UiO-66-NH<sub>2</sub> matches well with the reported patterns of the MOF (pattern b in Figure 2).<sup>53,60</sup> UiO-66-NH<sub>2</sub> is very stable during the loading of Pd precursor and the reduction treatment under 50 mL/min flow of 10% H<sub>2</sub>/Ar at 200 °C. We do not observe any obvious changes in the PXRD patterns of Pd@UiO-66-NH<sub>2</sub> that indicates the loss of the MOF's crystalline structure (pattern c



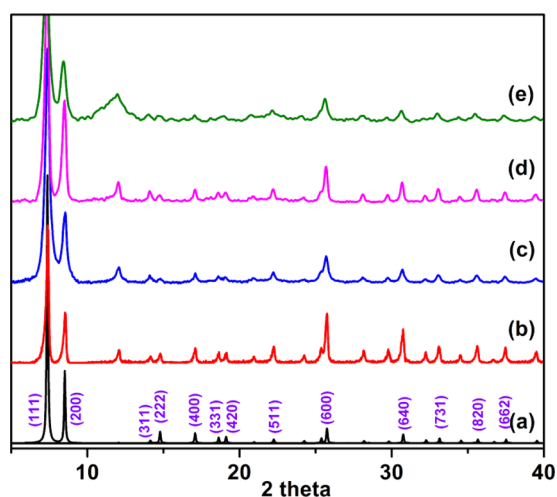


**Figure 2.** PXRD patterns of (a) simulated UiO-66, (b) as-synthesized UiO-66-NH<sub>2</sub>, (c) 2.0 wt % Pd@UiO-66-NH<sub>2</sub> after reduction, (d) 2.0 wt % Pd@UiO-66-NH<sub>2</sub> after reaction, (e) 2.0 wt % Pd@UiO-66-NH<sub>2</sub> after recycle test.

in Figure 2). Furthermore, we do not find any X-ray diffraction peaks from Pd nanocrystal, which suggests that the encapsulated Pd particles are very small. Thermogravimetric analysis (TGA) indicates that Pd@UiO-66-NH<sub>2</sub> is thermally stable below ~280 °C (Figure S3, Supporting Information).

The surface areas and pore volumes of the samples were measured by N<sub>2</sub> physisorption at -196 °C. Figure 3 shows the

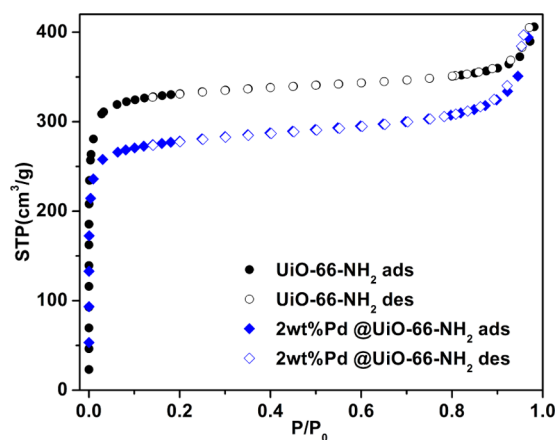


**Figure 3.** Nitrogen adsorption isotherms of the as-synthesized UiO-66-NH<sub>2</sub> and 2.0 wt % Pd@UiO-66-NH<sub>2</sub>.

N<sub>2</sub> adsorption–desorption isotherm profiles of UiO-66-NH<sub>2</sub> and 2.0 wt % Pd@UiO-66-NH<sub>2</sub>. All adsorption–desorption isotherms show a type I shape, a characteristic of microporous materials. As shown in Supporting Information, Table S1, the BET surface area and micropore volume of UiO-66-NH<sub>2</sub> were calculated to be 1194 m<sup>2</sup> g<sup>-1</sup> and 0.44 cm<sup>3</sup> g<sup>-1</sup>, respectively, which are close to the reported values.<sup>47</sup> Compared to UiO-66-NH<sub>2</sub>, the BET surface area and pore volume of 2.0 wt % Pd@UiO-66-NH<sub>2</sub> decreased to 936 m<sup>2</sup> g<sup>-1</sup> and 0.36 cm<sup>3</sup> g<sup>-1</sup>, respectively, mainly because of the occupation of the cages of UiO-66-NH<sub>2</sub> by Pd NCs.<sup>16</sup>

We also tried to determine the oxidation state of Pd in UiO-66-NH<sub>2</sub> after reduction using X-ray photoelectron spectroscopy (XPS). However, due to the overlap between Pd 3d and Zr 3p

peaks (from 330 to 350 eV) and the much higher concentration of Zr from the MOF compared to Pd, we could not get a good fitting of the XPS spectra to determine the oxidation state of the Pd (Figure S4, Supporting Information). Instead, we used extended X-ray absorption fine structure (EXAFS) spectroscopy to study the coordination environment of Pd before and after reducing the Pd(II)-loaded UiO-66-NH<sub>2</sub>. As shown in Figure 4a, the EXAFS spectrum of the sample before reduction is dominated by the Pd–O scattering. The Pd–O coordination number determined from fitting the EXAFS spectrum is  $3.6 \pm 0.3$  (Table S2, Supporting Information), which agrees with the structure of the Pd precursor, palladium acetate, although the interatomic distance ( $2.05 \pm 0.01$  Å) is slightly higher than that in Pd(OAc)<sub>2</sub> ( $2.00 \pm 0.01$  Å). After reduction with 10% H<sub>2</sub>/Ar at 200 °C, the scattering of Pd–Pd appears in Fourier transform, as shown in Figure 4b. EXAFS fitting showed that Pd–Pd scattering has a coordination number of  $3.7 \pm 0.3$  with interatomic distance of  $2.78 \pm 0.01$  Å, indicating the formation of Pd NCs.

Additionally, Fourier transform also indicates the presence of another scattering from Pd–N or Pd–O. The interatomic distance was found to be ~2.16–2.19 Å with fitting. This distance is obviously longer than that in PdO phase usually found in Pd catalysts (~2.0 Å).<sup>61,62</sup> However, in some catalysts with strong metal–support interaction, the metal–oxide distance was reported to be much longer (2.19 Å).<sup>63</sup> Besides, Pd–N bond length could vary between 2.0 and 2.2 Å, depending on the coordination environment.<sup>64,65</sup> Due to the presence of -NH<sub>2</sub> groups in UiO-66-NH<sub>2</sub>, it is more likely that the -NH<sub>2</sub> group coordinates with Pd NCs after the reduction.

The tandem oxidation-acetalization reactions of benzyl alcohol and ethylene glycol were carried out with 2.0 wt % Pd@UiO-66-NH<sub>2</sub> and 1.9 wt % Pd@UiO-66 under 0.1 MPa O<sub>2</sub> at 90 °C in cyclohexane. As shown in Table 1 (entry 1), Pd@UiO-66-NH<sub>2</sub> was an active catalyst for this one-pot tandem reaction and 99.9% conversion of benzyl alcohol with 99.9% selectivity to benzaldehyde ethylene acetal was achieved. On the contrary, UiO-66-NH<sub>2</sub> alone only gave 1.5% conversion of benzyl alcohol, which confirmed the oxidation of benzyl alcohol to benzaldehyde is catalyzed by Pd NCs. To confirm that the acetalization of benzaldehyde and ethylene glycol is catalyzed by UiO-66-NH<sub>2</sub>, we tested the activity of UiO-66-NH<sub>2</sub> in the acetalization reaction using benzaldehyde and ethylene glycol as the reactants. We found that the reaction reached 99.9% conversion and 99.9% selectivity after 6 h (Table 1, entry 3), which confirmed that UiO-66-NH<sub>2</sub> is a highly active and selective catalyst in the acetalization reaction. We also tested two control catalysts, 5.0 wt % Pd/C and 1.9 wt % Pd@UiO-66. We could not achieve high selectivity using Pd/C under the same reaction conditions (Table 1, entry 5). Using Pd@UiO-66, we obtained 91.0% conversion of benzyl alcohol and 95.0% selectivity to acetal (Table 1, entry 4), which are slightly lower than the respective values acquired on Pd@UiO-66-NH<sub>2</sub>. These catalysis results show the superiority of using MOFs as supports and also suggest that both Pd NCs and Lewis acid sites on MOFs are essential for the efficient tandem oxidation-acetalization reaction.

We also investigated the effect of solvent and found that cyclohexane is the best solvent for this tandem reaction (entries 1, 6, and 7 in Table 1). The high selectivity to benzaldehyde ethylene acetal in cyclohexane can be attributed to the low solubility of water in this nonpolar solvent. Because water is one of the products in the acetalization reaction, the low

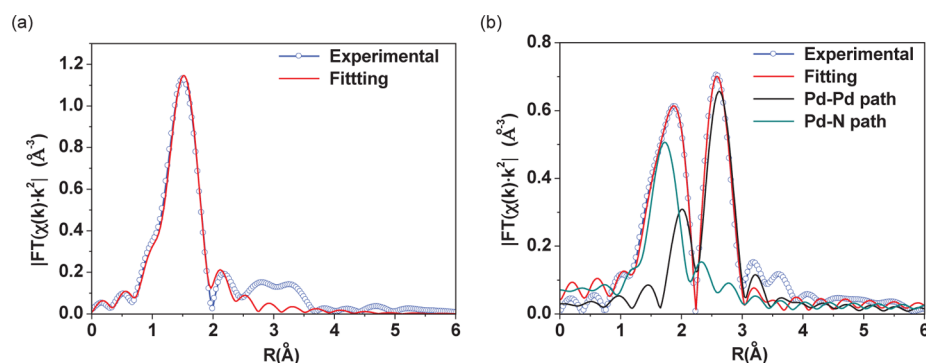
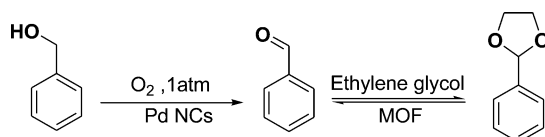


**Figure 4.** Fourier transform (FT) of EXAFS data extracted from Pd K edge (blue empty dot) and the computed fits (red line) in  $R$ -space for 4.8 wt % Pd@UiO-66-NH<sub>2</sub> samples: (a) before and (b) after reduction under 50 mL/min flow of 10% H<sub>2</sub>/Ar at 200 °C. FT peak positions are not corrected for phase shifts. The individual theoretical paths (Pd–Pd and Pd–N) used to fit the experimental data were also shown in (b). For comparison, only their magnitudes were shown.

**Table 1.** Performance of Different Catalysts in the Oxidation of Benzyl Alcohol and the Subsequent Acetalization with Ethylene Glycol

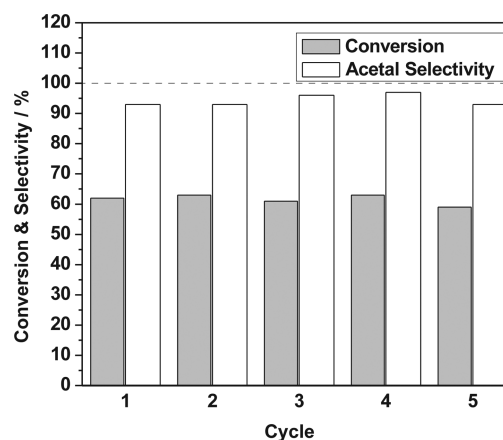


entry	sample	substrate	solvent	$t$ (h)	conv. (%)	alde (%)	acetal <sup>f</sup> (%)	ester <sup>g</sup> (%)
1 <sup>a</sup>	Pd@UiO-66-NH <sub>2</sub>	benzyl alcohol	cyclohexane	22	99.9		99.9	
2 <sup>b</sup>	UiO-66-NH <sub>2</sub>	benzyl alcohol	cyclohexane	22	1.5	54.1	45.9	
3 <sup>b,c</sup>	UiO-66-NH <sub>2</sub>	benzaldehyde	cyclohexane	6	99.9		99.9	
4 <sup>a</sup>	Pd@UiO-66	benzyl alcohol	cyclohexane	22	91.0	5.0	95.0	
5 <sup>d</sup>	Pd/C	benzyl alcohol	cyclohexane	22	99.0	40.3	59.7	
6 <sup>e</sup>	Pd@UiO-66-NH <sub>2</sub>	benzyl alcohol	ethylene glycol	3	99.9	6.2	59.2	30.6
7 <sup>e</sup>	Pd@UiO-66-NH <sub>2</sub>	benzyl alcohol	toluene	22	98.7	45.9	54.1	

<sup>a</sup>Reaction conditions: 90 °C, 0.1 MPa O<sub>2</sub>, benzyl alcohol (0.1 mmol), ethylene glycol (100  $\mu$ L, 1.8 mmol), cyclohexane (2 mL), 5 mg 2.0 wt % Pd@MOF, metal/substrate = 1:100. <sup>b</sup>4.9 mg of UiO-66-NH<sub>2</sub> was used. <sup>c</sup>0.1 mmol benzaldehyde was used. <sup>d</sup>2 mg of 5%Pd/C was used. <sup>e</sup>2 mL of solvent was used. <sup>f</sup>Benzaldehyde ethylene acetal. <sup>g</sup>2-hydroxyethyl benzoate.

solubility of water in the reaction solvent could shift the equilibrium of the reaction to the acetalization product.<sup>66</sup> Furthermore, it is noteworthy that we did not detect any benzoic acid or the corresponding ester after the designated reaction time when we used cyclohexane as the reaction solvent, which shows the superior selectivity of Pd@UiO-66-NH<sub>2</sub> under appropriate reaction conditions. The inhibition of the further oxidation of benzaldehyde could also be attributed to the low solubility of water in cyclohexane. The oxidation of alcohols to carboxylic acid normally proceeds through an aldehyde hydrate (R–CH(OH)<sub>2</sub>), which can be further oxidized to the carboxylic acid.<sup>67,68</sup> Because water is expelled from the cyclohexane, carboxylic acid cannot be formed. To explore the effect of Pd loading on the activity and selectivity of the tandem reaction, we synthesized Pd@UiO-66-NH<sub>2</sub> with 1.0, 2.0, and 4.0 wt % Pd. At the same metal to substrate ratio (1 mol %), the catalysts with higher Pd loading show higher conversion (Table S3, Supporting Information), which means the catalysts with higher Pd loading are more active and give higher turnover frequencies.

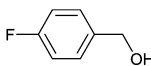
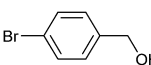
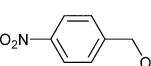
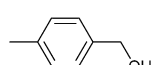
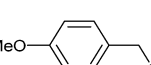
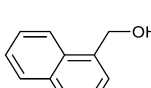
The reusability of the Pd@UiO-66-NH<sub>2</sub> and Pd@UiO-66 catalyst were also examined. After an initial reaction, the solid catalyst was isolated from the liquid phase by centrifugation and then reused in additional runs. The Pd@UiO-66-NH<sub>2</sub> catalyst could be recycled at least five times (Figure 5). However, Pd@UiO-66 deactivated in the third recycle run (Figure S6,



**Figure 5.** Recycling test with 2.0 wt % Pd@UiO-66-NH<sub>2</sub> catalyst. Reaction conditions: Cyclohexane (2 mL), benzyl alcohol (0.1 mmol), ethylene glycol (100  $\mu$ L), 5 mg of 2.0 wt % Pd@UiO-66-NH<sub>2</sub>, metal/substrate = 1:100, 0.1 MPa O<sub>2</sub>, reflux at 90 °C for 6 h.

Supporting Information). We also observed more severe aggregation of Pd NCs in UiO-66 (Figure S7, Supporting Information) after reaction compared to those in UiO-66-NH<sub>2</sub> (Figure S5, Supporting Information), which indicates UiO-66-NH<sub>2</sub> is a better support for Pd NCs. The conversion was controlled at below 70% because complete conversion could

Table 2. Tandem Oxidation-Acetalization Reaction of Various Substituted Benzyl Alcohols Catalyzed by Pd@UiO-66-NH<sub>2</sub><sup>a</sup>

Entry	Substrates	t (h)	Conv. (%)	Acetal (%)	Aldehyde (%)
1		48	17.4	100	0
2		48	5.60	16.2	83.8
3		48	35.3	78.8	21.2
4		48	73.3	94.8	5.2
5		48	99.9	99.0	1.0
6		48	50.3	62.0	38.0

<sup>a</sup>Reaction conditions: 90 °C, 0.1 MPa O<sub>2</sub>, substituted benzyl alcohol (0.1 mmol), ethylene glycol (100 μL, 1.8 mmol), cyclohexane (2 mL), 5 mg of 2.0 wt % Pd@UiO-66-NH<sub>2</sub>, metal/substrate = 1 mol %.

mask the deactivation of the catalyst.<sup>69</sup> The BET surface area of the used Pd@UiO-66-NH<sub>2</sub> decreased from 936 m<sup>2</sup> g<sup>-1</sup> to 828 m<sup>2</sup> g<sup>-1</sup> (Figure S8, Supporting Information), which may be due to the residual reactants or products trapped inside the UiO-66-NH<sub>2</sub>. Furthermore, we measured the PXRD pattern of the used catalysts and found the crystalline structure of the UiO-66-NH<sub>2</sub> was still maintained after the fifth cycle (pattern e in Figure 2). TEM images of used Pd@UiO-66-NH<sub>2</sub> catalysts only show slight aggregation of Pd NCs (Figure S5, Supporting Information), which does not affect the activity of the catalysts within five recycle runs.

The scope of the tandem catalytic system was investigated by performing the oxidation-acetalization reaction of various substituted benzyl alcohols. Table 2 summarizes the results of these tandem reactions. We found that benzyl alcohols with electron-withdrawing groups like fluoro and bromo gave low conversion and/or selectivity, whereas electron-donating groups (-OCH<sub>3</sub> and -CH<sub>3</sub>) showed moderate to high conversion and selectivity to the corresponding acetals. We used Hammett's equation to obtain the correlation between substituent constant and reaction rate (Figure S9, Supporting Information). The negative value of ρ (-4.07) indicates the tandem reaction is facilitated by the high electron density at the reaction center. Currently, we are studying bimetallic NCs encapsulated in this MOF for oxidation of aliphatic alcohols.

In order to confirm the heterogeneity of the catalyst, the hot filtration test was carried out by stopping the tandem reaction after 90 min. The reaction reached 57% conversion and 90% selectivity to benzaldehyde ethylene acetal. The reaction solution was removed quickly from the solid catalyst and was transferred to another flask under the same reaction conditions. No further increase in either the conversion of benzyl alcohol or the selectivity to benzaldehyde ethylene acetal was observed in the transferred solution after the solid catalyst was removed (Figure 6). These results demonstrate that the active sites for both the oxidation and the acetalization reactions were on the

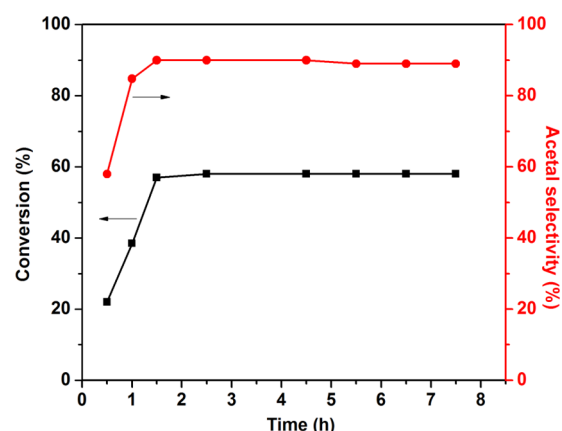


**Figure 6.** Leaching test for the tandem reaction of benzyl alcohol with ethylene glycol over 2.0 wt % Pd@UiO-66-NH<sub>2</sub>. Reaction conditions: benzyl alcohol (0.1 mmol), ethylene glycol (100 μL), mesitylene (8 μL), cyclohexane (2 mL), 2.0 wt % Pd@UiO-66-NH<sub>2</sub>, substrate/metal = 100, reflux at 90 °C. The solid catalyst was filtered from the reaction solution after 90 min, whereas the filtrate was transferred to a new vial and reaction was carried out under identical conditions for an additional 8 h.

solid catalyst, and there are no leached active species under the reaction conditions.

#### 4. CONCLUSIONS

We have developed a heterogeneous tandem catalyst for the oxidation of benzyl alcohol and the subsequent acetalization with ethylene glycol catalyzed by UiO-66-NH<sub>2</sub> supported Pd nanoclusters. This bifunctional Pd@UiO-66-NH<sub>2</sub> catalyst exhibits high selectivity to give acetal products in this tandem oxidation-acetalization reaction and can be reused five times without any loss in activity and selectivity. On the contrary, Pd@UiO-66 showed deactivation at the third recycle run and more severe aggregation of Pd NCs was observed. We also found that using the nonpolar solvent, cyclohexane, is essential

for the high selectivity to acetal, which could promote the acetalization reaction and prevent the further oxidation of aldehydes to the corresponding esters. This work demonstrates the potential of MOF-based catalysts in tandem heterogeneous catalysis. Under appropriate conditions, both high selectivity and stability of MOF-based catalysts can be achieved. Further work on exploring new tandem catalytic reactions with these catalytic systems and optimizing the performance of the multifunctional MOFs via preparing bimetallic nanoclusters is currently underway.

## ■ ASSOCIATED CONTENT

### Supporting Information

EDX, EXAFS, XPS, nitrogen sorption and TGA measurements; TEM images for the catalyst after reaction. This material is available free of charge via the Internet at <http://pubs.acs.org>.

## ■ AUTHOR INFORMATION

### Corresponding Author

\*E-mail: [whuang@iastate.edu](mailto:whuang@iastate.edu).

### Author Contributions

<sup>‡</sup>X.L. and Z.G. contributed equally. The manuscript was written through contributions of all authors. All authors have given approval to the final version of the manuscript.

### Notes

The authors declare no competing financial interest.

## ■ ACKNOWLEDGMENTS

We thank Ames Laboratory (Royalty Account) and Iowa State University for startup funds. This work was also supported by the Laboratory Research and Development Program of The Ames Laboratory. The Ames Laboratory is operated for the U.S. Department of Energy by Iowa State University under Contract No. DE-AC02-07CH11358. We thank to Dale L. Brewster, Steve M. Heald, Trudy B. Bolin, Tianpin Wu, and Jeff Miller for the help during XAS measurement at APS. Use of the Advanced Photon Source, an Office of Science User Facility operated for the U.S. Department of Energy (DOE) Office of Science by Argonne National Laboratory, was supported by the U.S. DOE under Contract No. DE-AC02-06CH11357. We thank Robert J. Angelici for his advice during the writing of this manuscript. We thank Gordon J. Miller for use of PXRD, Brent Shanks for use of TGA, and Igor I. Slowing for use of gas adsorption analyzer and ICP-AES.

## ■ REFERENCES

- (1) Shiju, N. R.; Alberts, A. H.; Khalid, S.; Brown, D. R.; Rothenberg, G. *Angew. Chem., Int. Ed.* **2011**, *50*, 9615–9619.
- (2) Grondal, C.; Jeanty, M.; Enders, D. *Nat. Chem.* **2010**, *2*, 167–178.
- (3) Shin, J. Y.; Jung, D. J.; Lee, S.-g. *ACS Catal.* **2013**, *3*, 525–528.
- (4) Guan, Y.; Zhang, D.; Wang, Y. *Catal. Lett.* **2012**, *142*, 1225–1233.
- (5) Kim, J. H.; Lee, S.-g. *Org. Lett.* **2011**, *13*, 1350–1353.
- (6) Shylesh, S.; Wagener, A.; Seifert, A.; Ernst, S.; Thiel, W. R. *Angew. Chem., Int. Ed.* **2010**, *49*, 184–187.
- (7) Nicolaou, K. C.; Edmonds, D. J.; Bulger, P. G. *Angew. Chem., Int. Ed.* **2006**, *45*, 7134–7186.
- (8) Yang, G.; Kawata, H.; Lin, Q.; Wang, J.; Jin, Y.; Zeng, C.; Yoneyama, Y.; Tsubaki, N. *Chem. Sci.* **2013**, *4*, 3958–3964.
- (9) Zhou, H.-C.; Long, J. R.; Yaghi, O. M. *Chem. Rev.* **2012**, *112*, 673–674.
- (10) Betard, A.; Fischer, R. A. *Chem. Rev.* **2012**, *112*, 1055–1083.

- (11) Getman, R. B.; Bae, Y.-S.; Wilmer, C. E.; Snurr, R. Q. *Chem. Rev.* **2012**, *112*, 703–723.
- (12) Horcajada, P.; Gref, R.; Baati, T.; Allan, P. K.; Maurin, G.; Couvreur, P.; Ferey, G.; Morris, R. E.; Serre, C. *Chem. Rev.* **2012**, *112*, 1232–1268.
- (13) Kreno, L. E.; Leong, K.; Farha, O. K.; Allendorf, M.; Van Duyne, R. P.; Hupp, J. T. *Chem. Rev.* **2012**, *112*, 1105–1125.
- (14) Farrusseng, D.; Aguado, S.; Pinel, C. *Angew. Chem., Int. Ed.* **2009**, *48*, 7502–7513.
- (15) Jiang, H.-L.; Akita, T.; Ishida, T.; Haruta, M.; Xu, Q. *J. Am. Chem. Soc.* **2011**, *133*, 1304–1306.
- (16) Aijaz, A.; Karkamkar, A.; Choi, Y. J.; Tsumori, N.; Rönnebro, E.; Autrey, T.; Shioyama, H.; Xu, Q. *J. Am. Chem. Soc.* **2012**, *134*, 13926–13929.
- (17) Zhu, Q.-L.; Li, J.; Xu, Q. *J. Am. Chem. Soc.* **2013**, *135*, 10210–10213.
- (18) Li, P.-Z.; Aranishi, K.; Xu, Q. *Chem. Commun.* **2012**, *48*, 3173–3175.
- (19) Yadav, M.; Xu, Q. *Chem. Commun.* **2013**, *49*, 3327–3329.
- (20) Liu, H.; Liu, Y.; Li, Y.; Tang, Z.; Jiang, H. J. *Phys. Chem. C* **2010**, *114*, 13362–13369.
- (21) Dhakshinamoorthy, A.; Garcia, H. *Chem. Soc. Rev.* **2012**, *41*, 5262–5284.
- (22) Hermannsdoerfer, J.; Kempe, R. *Chem.—Eur. J.* **2011**, *17*, 8071–8077.
- (23) Gu, X.; Lu, Z.-H.; Jiang, H.-L.; Akita, T.; Xu, Q. *J. Am. Chem. Soc.* **2011**, *133*, 11822–11825.
- (24) Esken, D.; Turner, S.; Lebedev, O. I.; Van Tendeloo, G.; Fischer, R. A. *Chem. Mater.* **2010**, *22*, 6393–6401.
- (25) Ishida, T.; Nagaoka, M.; Akita, T.; Haruta, M. *Chem.—Eur. J.* **2008**, *14*, 8456–8460.
- (26) Cirujano, F. G.; Llabres i Xamena, F. X.; Corma, A. *Dalton Trans.* **2012**, *41*, 4249–4254.
- (27) Pan, Y.; Yuan, B.; Li, Y.; He, D. *Chem. Commun.* **2010**, *46*, 2280–2282.
- (28) Liu, H.; Chen, G.; Jiang, H.; Li, Y.; Luque, R. *ChemSusChem* **2012**, *5*, 1892–1896.
- (29) Liu, H.; Li, Y.; Jiang, H.; Vargas, C.; Luque, R. *Chem. Commun.* **2012**, *48*, 8431–8433.
- (30) Zhao, M.; Deng, K.; He, L.; Liu, Y.; Li, G.; Zhao, H.; Tang, Z. *J. Am. Chem. Soc.* **2014**, *136*, 1738–1741.
- (31) Dhakshinamoorthy, A.; Opanasenko, M.; Cejka, J.; Garcia, H. *Catal. Sci. Technol.* **2013**, *3*, 2509–2540.
- (32) Thavornprasert, K.-a.; Capron, M.; Jalowiecki-Duhamel, L.; Gardoll, O.; Trentesaux, M.; Mamede, A.-S.; Fang, G.; Faye, J.; Touati, N.; Vezin, H.; Dubois, J.-L.; Couturier, J.-L.; Dumeignil, F. *Appl. Catal., B* **2014**, *145*, 126–135.
- (33) Liu, H.; Iglesia, E. *J. Phys. Chem. B* **2003**, *107*, 10840–10847.
- (34) Liu, H.; Iglesia, E. *J. Phys. Chem. B* **2004**, *109*, 2155–2163.
- (35) Secordel, X.; Yoboue, A.; Cristol, S.; Lancelot, C.; Capron, M.; Paul, J.-F.; Berrier, E. *J. Solid State Chem.* **2011**, *184*, 2806–2811.
- (36) Yuan, Y. Z.; Liu, H. C.; Imoto, H.; Shido, T.; Iwasawa, Y. *J. Catal.* **2000**, *195*, 51–61.
- (37) Chan, A. S. Y.; Chen, W.; Wang, H.; Rowe, J. E.; Madey, T. E. *J. Phys. Chem. B* **2004**, *108*, 14643–14651.
- (38) Fu, Y.; Shen, J. *Chem. Commun.* **2007**, 2172–2174.
- (39) Chen, S.; Wang, S.; Ma, X.; Gong, J. *Chem. Commun.* **2011**, *47*, 9345–9347.
- (40) Liu, J.; Fu, Y.; Sun, Q.; Shen, J. *Microporous Mesoporous Mater.* **2008**, *116*, 614–621.
- (41) Tanaka, T.; Takenaka, S.; Funabiki, T.; Yoshida, S. In *Acid-Base Catalysis II*, Proceedings of the International Symposium on Acid-Base Catalysis II; Hattori, H.; Misono, M.; Ono, Y., Eds.; Vol. 90; Elsevier: Amsterdam, 1994; pp 485–490.
- (42) Tanaka, T.; Takenaka, S.; Funabiki, T.; Yoshida, S. *Chem. Lett.* **1994**, 809–812.
- (43) Heitler, C.; Scaife, D. B.; Thompson, B. W. *J. Chem. Soc. A* **1967**, 1409–1413.



- (44) Bueno, A. C.; Goncalves, J. A.; Gusevskaya, E. V. *Appl. Catal., A* **2007**, *329*, 1–6.
- (45) Smith, B. M.; Graham, A. E. *Tetrahedron Lett.* **2007**, *48*, 4891–4894.
- (46) Kim, M.; Cohen, S. M. *CrystEngComm* **2012**, *14*, 4096–4104.
- (47) Vermoortele, F.; Ameloot, R.; Vimont, A.; Serre, C.; De Vos, D. *Chem. Commun.* **2011**, *47*, 1521–1523.
- (48) Vermoortele, F.; Vandichel, M.; Van de Voorde, B.; Ameloot, R.; Waroquier, M.; Van Speybroeck, V.; De Vos, D. E. *Angew. Chem., Int. Ed.* **2012**, *51*, 4887–4890.
- (49) Timofeeva, M. N.; Panchenko, V. N.; Jun, J. W.; Hasan, Z.; Matrosova, M. M.; Jhung, S. H. *Appl. Catal., A* **2014**, *471*, 91–97.
- (50) Silva, P. H. R.; Goncalves, V. L. C.; Mota, C. J. A. *Bioresour. Technol.* **2010**, *101*, 6225–6229.
- (51) Ray, R.; Chowdhury, A. D.; Lahiri, G. K. *ChemCatChem* **2013**, *5*, 2158–2161.
- (52) Ajaikumar, S.; Pandurangan, A. *J. Mol. Catal. A: Chem.* **2008**, *290*, 35–43.
- (53) Cavka, J. H.; Jakobsen, S.; Olsbye, U.; Guillou, N.; Lamberti, C.; Bordiga, S.; Lillerud, K. P. *J. Am. Chem. Soc.* **2008**, *130*, 13850–13851.
- (54) Newville, M. *J. Synchrotr. Radiat.* **2001**, *8*, 322–324.
- (55) Ravel, B.; Newville, M. *J. Synchrotr. Radiat.* **2005**, *12*, 537–541.
- (56) Rehr, J. J.; Kas, J. J.; Prange, M. P.; Sorini, A. P.; Takimoto, Y.; Vila, F. C. *R. Phys.* **2009**, *10*, 548–559.
- (57) Ravel, B.; Newville, M. *Phys. Scr.* **2005**, *2005*, 1007–1010.
- (58) Zabinsky, S. L.; Rehr, J. J.; Ankudinov, A.; Albers, R. C.; Eller, M. *J. Phys. Rev. B* **1995**, *52*, 2995–3009.
- (59) Guo, Z.; Xiao, C.; Maligal-Ganesh, R. V.; Zhou, L.; Goh, T. W.; Li, X.; Tesfagaber, D.; Thiel, A.; Huang, W. *ACS Catal.* **2014**, *4*, 1340–1348.
- (60) Valenzano, L.; Civalleri, B.; Chavan, S.; Bordiga, S.; Nilsen, M. H.; Jakobsen, S.; Lillerud, K. P.; Lamberti, C. *Chem. Mater.* **2011**, *23*, 1700–1718.
- (61) Gaudet, J. R.; de la Riva, A.; Peterson, E. J.; Bolin, T.; Dadye, A. K. *ACS Catal.* **2013**, *3*, 846–855.
- (62) Cho, S. J.; Kang, S. K. *J. Phys. Chem. B* **2000**, *104*, 8124–8128.
- (63) Kampers, F. W. H.; Koningsberger, D. C. *Faraday Discuss.* **1990**, *89*, 137–141.
- (64) Harkness, M. B.; Alvarado, E.; Badaj, A. C.; Skrela, B. C.; Fan, L.; Lavoie, G. G. *Organometallics* **2013**, *32*, 3309–3321.
- (65) Albrecht, M.; Stoeckli-Evans, H. *Chem. Commun.* **2005**, 4705–4707.
- (66) Liu, C.-H.; Yu, X.-Y.; Liang, X.-Z.; Wang, W.-J.; Yang, J.-G.; He, M.-Y. *Chin. J. Chem.* **2007**, *25*, 83–85.
- (67) Schmidt, A.-K. C.; Stark, C. B. W. *Org. Lett.* **2011**, *13*, 4164–4167.
- (68) Noyori, R.; Aoki, M.; Sato, K. *Chem. Commun.* **2003**, 1977–1986.
- (69) Jones, C. *Top. Catal.* **2010**, *53*, 942–952.